Hindawi Publishing Corporation
Journal of Nanomaterials
Volume 2016, Article ID 6581691, 11 pages
http://dx.doi.org/10.1155/2016/6581691

*Research Article*

# $TiO_2$-CdS Nanocomposites: Effect of CdS Oxidation on the Photocatalytic Activity

**A. Hamdi,[1] D. P. Ferreira,[2] A. M. Ferraria,[2] D. S. Conceição,[2] L. F. Vieira Ferreira,[2] A. P. Carapeto,[2] S. Boufi,[3] S. Bouattour,[1] and A. M. Botelho do Rego[2]**

[1]*Laboratoire de Chimie Inorganique, Faculté des Sciences de Sfax, Université de Sfax, BP 1171, 3000 Sfax, Tunisia*
[2]*Centro de Química-Física Molecular and Institute of Nanoscience and Nanotechnology, Instituto Superior Técnico, Universidade de Lisboa, 1049-001 Lisbon, Portugal*
[3]*LSME, Faculté des Sciences de Sfax, Université de Sfax, BP 1171, 3018 Sfax, Tunisia*

Correspondence should be addressed to S. Bouattour; soraa.boufi@yahoo.com
and A. M. Botelho do Rego; amrego@tecnico.ulisboa.pt

Received 20 July 2016; Accepted 28 September 2016

Academic Editor: Domenico Acierno



Nanocomposites $TiO_2$-CdS with different relative contents of CdS (molar ratios Cd/Ti = 0.02, 0.03, 0.05, 0.1, 0.2, and 0.5) were studied. The structural, photophysical, and chemical properties were investigated using XRD, Raman spectroscopy, XPS, GSDR, and LIL. XRD and Raman results confirmed the presence of $TiO_2$ and CdS with intensities dependent on the ratio Cd/Ti. The presence of $CdSO_4$ was detected by XPS at the surface of all $TiO_2$-CdS composites. The relative amount of sulphate was dependent on the CdS loading. Luminescence time-resolved spectra clearly proved the existence of an excitation transfer process from CdS to $TiO_2$ through the luminescence emission from $TiO_2$ after excitation of CdS at $\lambda_{exc}$ = 410 nm, where no direct excitation of $TiO_2$ occurs. Photodegradation of a series of aromatic carboxylic acids—benzoic, salicylic, 4-bromobenzoic, 3-phenylpropionic, and veratric acids—showed a great enhancement in the photocatalytic efficiency of the $TiO_2$-CdS composites, which is due, mainly, to the effect of the charge carriers' increased lifetime. In addition, it was shown that the oxidation of CdS to $CdSO_4$ did not result in the deactivation of the photocatalytic properties and even contributed to enhance the degradation efficiency.

## 1. Introduction

In the past years, great interest has been focused on the research and development of water treatment methodologies due to the increasing presence of harmful pollutants in wastewater effluents [1, 2]. It has been shown recently that the efficiency of pollutants photodegradation is mainly determined by the properties of the photocatalysts [3, 4]. The importance of selecting suitable photocatalysts which have the capacity of absorbing solar visible light and the ability to separate photoexcited electrons from the holes have been emphasized. Among the reported semiconductor photocatalysts, titanium dioxide has attracted worldwide interest due to its strong oxidation activity and stability. In recent years, because of the band gap value (3.2 eV) in the UV light range, the modification of $TiO_2$ photocatalysts for the enhancement of light absorption and photocatalytic activity under visible light irradiation became the main research direction. To reach this goal, several modification techniques that exist mainly involve doping $TiO_2$ with metals or nonmetal elements such as Fe, Cu, C, and S [5–8], sensitization of $TiO_2$ by adsorbed dyes [9, 10], and coupling $TiO_2$ with semiconductors having lower band gaps and more cathodic conduction band (CB) [11, 12].

CdS is a semiconductor with a bandgap of 2.4 eV. Its excitation wavelength is ≤ 518 nm and it has obvious advantages in absorbing within the solar spectrum. So, not only are the $TiO_2$-CdS composite nanoparticles excited easily by visible light, but also the recombination probabilities of the photoelectron-hole pairs are diminished [13, 14]. Bessekhouad et al. [14] found that under visible illumination the coupled CdS-$TiO_2$ exhibit faster degradation rate than both isolated components of the composite photocatalyst. Serpone et al. [15] reported for the first time the photocatalysed oxidation of

several phenol-based molecules by coupled semiconductors suspension in which the beneficial effect of the charge transfer was clearly demonstrated. They mentioned that in addition to the flat band potential of the components the photocatalytic performance of the coupled semiconductors is also related to the geometry of the particles, the surface contact between particles, and the particle sizes. These parameters strongly depend on the preparation method [15]. However, as widely recognized, there are several disadvantages concerning both the preparation and the utilization of such "coupled" systems. Specially, the oxidation of $S^{2-}$ to $S^{6+}$ in CdS semiconductor in the presence of air has been considered for a long time as an inevitable problem which causes uncertainty in the quality of the product and troublesome for the synthesis. The oxidation usually occurs as follows [16, 17]:

$$CdS + 2O_2 \longrightarrow Cd^{2+} + SO_4^{2-} \quad (1)$$

Therefore, many research groups considered that it is highly desirable to find new approaches that are capable of overcoming the above problems associated with the preparation of nanosized "coupled" CdS-$TiO_2$ photocatalysts. Some attempts have already been made by Zou and coworkers [18]. They successfully deposited CdS on the surface of $TiO_2$ using SILAR process for the CdS immobilization. Recently, Wang et al. [19] reported a simple and straightforward method for obtaining CdS coupled $TiO_2$ hydrosol with competitive physicochemical and photochemical properties. It was based on a microemulsion-mediated solvothermal hydrolysis of tetrabutyltitanate. However, some other studies reported a beneficial effect of $SO_4^{2-}$ produced upon CdS oxidation. In particular, Colón et al. [20] demonstrated that $SO_4^{2-}$ plays an important role in the photocatalytic oxidation reaction using $SO_4^{2-}/TiO_2$ catalyst. Sulphate ions increase the adsorption strength of the pollutant to the surface of catalysts which contributes to the improvement of photocatalytic activity. Moreover, Fu et al. [21] reported that the conversion of $CH_3Br$ over sulphated $TiO_2$ was six times higher than that over $TiO_2$.

From the above cited references, associating CdS to $TiO_2$ is expected to improve the photodegradation activity since it permits to avoid unwanted charge recombination and to enlarge the light response of $TiO_2$ to visible light.

In the present study, $TiO_2$-CdS samples have been prepared by suspension mixing followed by annealing at 400°C, in order (i) to exploit the optical absorption properties of CdS in the visible energy range and (ii) to increase the surface contact between CdS and $TiO_2$ nanoparticles. The photodegradation of carboxylic acids in aerated conditions served as reference tests for the evaluation of the photocatalytic activity of the prepared $TiO_2$-CdS nanocomposites. The effect of $SO_4^{2-}$ ions on the photocatalytic activity was also investigated and is an innovative aspect of this study.

## 2. Materials and Methods

*2.1. Materials.* Titanium(IV) oxide, anatase nanopowder, <25 nm particle size, 99.7% trace metals basis, CdS powder, 99.995% trace metals basis, ethanol absolute ≥99.8%, benzoic, salicylic, 4-bromobenzoic, 3-phenylpropionic, and veratric acids were all purchased from Aldrich.

*2.2. Preparation of CdS-Doped $TiO_2$.* $TiO_2$-$X$CdS nanocomposites with different contents of CdS were prepared and the resulting samples were noted as $TiO_2$-$X$CdS, where $X$ is the molar ratio Cd/Ti ($X$ = 0.02, 0.03, 0.05, 0.1, 0.2, and 0.5). $TiO_2$ nanoparticles were immersed in a suspension of CdS nanoparticles in ethanol. $TiO_2$-CdS powders were dried at ambient temperature for 24 h and, then, annealed at 400°C.

*2.3. X-Ray Diffraction Analysis.* The X-ray diffraction (XRD) patterns were performed using an X-ray Siemens/D5000 diffractometer with $CuK_\alpha$ radiation. The scanning range ($2\theta$) was from 20° to 75° with a scanning rate of 0.5°/min.

*2.4. Ground State Diffuse Reflectance Absorption Spectra (GSDR).* Ground state absorption studies were performed using a homemade diffuse reflectance laser flash photolysis setup, with a 250 W Halogen lamp as monitoring lamp and in this way recording the lamp profile for all samples under study and also for two standards, barium sulphate powder and a Spectralon disk. A fixed monochromator coupled to an ICCD with time gate capabilities was used for detecting the reflectance signals. The reflectance, $R$, from each sample was obtained in the UV-Vis-NIR spectral regions and the remission function, $F(R)$, was calculated using the Kubelka-Munk equation for optically thick samples. The remission function is $F(R) = (1 - R)^2/2R$. Details regarding the data treatment can be found in [22] and references quoted therein.

*2.5. Raman Spectroscopy.* $\mu$-Raman measurements were carried out in a backscattering microconfiguration, with a homemade apparatus with a Cobolt Samba CW DPSSL, 300 mW, and 532 nm as the excitation source, coupled to a BX-FM microscope from Olympus equipped with 10x, 50x, or 100x Olympus LWD objectives. The laser beam was focused on a diameter of about 25, 5, and 1.5–2 $\mu$m, respectively. The Raman probe was coupled to a Shamrock 163 spectrograph (Andor, with a 100 $\mu$m entrance slit) and a Newton DU 971P-BV camera from Andor was used as detector for the Raman signals, working at –60°C [23].

*2.6. Laser Induced Luminescence, LIF, and LIP.* The setup for time-resolved luminescence LIL (laser induced fluorescence, LIF, and laser induced phosphorescence, LIP) is presented in [22]. The light arising from the irradiation of solid samples with the laser pulse is collected by a collimating beam probe coupled to an optical fiber (fused silica) and is detected by a gated intensified charge coupled device Andor, model i-Star 720. The ICCD is coupled to a fixed imaging compact spectrograph (Andor, model Shamrock 263). The system can be used either by capturing all light emitted by the sample or in a time-resolved mode by using the ICCD delay unit. The ICCD has high speed gating electronics (2.3 ns) and intensifier and covers the 250–900 nm wavelength range.

Time-resolved emission spectra were performed in the nanosecond to second time range either with a $N_2$ laser

(excitation wavelength, $\lambda_{exc}$ = 337 nm, PTI model 2000, *ca.* 600 ps FWHM, about 1 mJ per pulse) or using a dye laser coupled to the $N_2$ ($\lambda_{exc}$ = 410 nm, using the PLD400 from PTI as laser dye). Emission spectra were obtained at 77 K, due to the fact that the room temperature luminescence intensity is negligible for the anatase form of $TiO_2$. In all cases under study only the initial 1 $\mu$s part of the decay was analysed.

*2.7. X-Ray Photoelectron Spectroscopy.* For the chemical characterization, a Kratos XSAM800 XPS spectrometer and nonmonochromatic Al K$\alpha$ radiation, without any flood gun for charge correction, were used. Typical operating conditions were 12 kV, 10 mA (120 W), and a pressure in the range of $10^{-7}$ Pa. Charge shifts were corrected taking, as references, the binding energy (BE) of aliphatic carbons centred at 285.0 eV for the CdS sample and the BE of Ti $2p_{3/2}$ in $TiO_2$, centred at 458.8 eV [24], for the $TiO_2$-*X*CdS samples. The detailed XPS regions were analysed and fitted using Gaussian and Lorentzian function products. Shirley backgrounds and source satellites were subtracted from spectra. Data treatment was performed with the help of XPS Peak 4.1 software package (freeware). For quantitative purposes, sensitivity factors were C 1s: 0.25; O 1s: 0.66; S 2p: 0.54; Cd $3d_{5/2}$: 3.48; Ti 2p: 1.76.

*2.8. Evaluation of the Photodegradation Processes.* The photocatalytic performance of $TiO_2$-*X*CdS samples with different CdS loadings was evaluated by following the absorption spectra, as a function of time, of organic pollutants solutions. For photodegradation tests, different organic compounds were selected and used as pollutant models ($c = 5 \times 10^{-4}$ M) in the presence of $TiO_2$-*X*CdS and exposed to visible irradiation. Organic pollutants selected were chosen to be not volatile, they can be analysed by UV absorption spectroscopy, and their solubility is larger than $10^{-4}$ mol/L. The maximum absorbance, corresponding to the remaining concentration of the pollutant in solution, was recorded at constant time intervals of 1 h during 6 to 8 h by UV/vis spectroscopy. The UV-visible absorbance spectra were obtained using a Cecil UV-visible spectrophotometer in the range 200–800 $cm^{-1}$.

The UV absorbance of the solutes was measured at their corresponding $\lambda_{max}$ (which are situated, in this work, between 240 and 290 nm). Calibration curves were previously established for each solute here studied.

Each sample was stored in the dark for 1 h (before irradiation) to reach the adsorption equilibrium. The adsorbed amount of solute in the dark was lower than 6% for all the samples. The set of degradation experiences was carried out under irradiation by a light source emitting only visible light. A 42 W Halogen lamp power (230 V) was used as a source of irradiation. The use of a lamp is very important to have constant intensity and overcome fluctuations in solar intensity due to the season or the time of day.

## 3. Results and Discussion

*3.1. XRD Analysis.* The crystal structure of the $TiO_2$-*X*CdS samples was examined by X-ray diffraction analysis. All the spectra are qualitatively similar and Figure 1 shows the XRD pattern for the sample $TiO_2$-0.2CdS. Two distinct reflections attributed to the anatase form of $TiO_2$ are observed at 25.6° and 48°. They can be attributed to (101) and (200) crystal planes [25]. Additionally, the XRD patterns of these samples showed four other reflections at 25.1°; 27.1°; 28.8°; 43.8°; and 52.0° which can be assigned to the CdS hexagonal wurtzite phase (100), (002), (101), (110), and (112) crystal planes, respectively [26]. No other forms of $TiO_2$ or CdS were observed in the studied samples. As a result, the XRD patterns clearly show that $TiO_2$ anatase and CdS wurtzite coexisted.

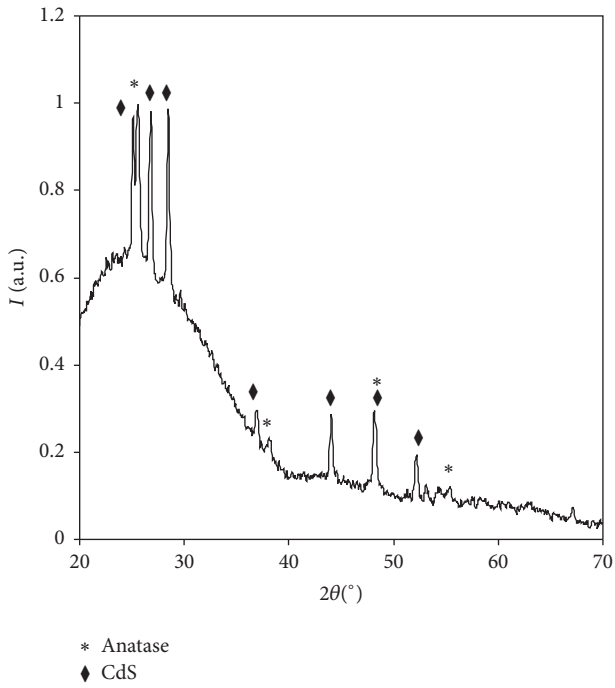


Figure 1: XRD pattern of $TiO_2$-0.2CdS sample.

*3.2. Ground State Diffuse Reflectance Absorption Studies (GSDR).* In Figure 2, we can see the ground state diffuse reflectance spectra of samples with different relative amounts of dopant. $TiO_2$ nanoparticles and CdS powder spectra are also included for comparison. The first conclusion is that the composite spectra are superpositions of the individual spectra of $TiO_2$ and CdS exhibiting 2 distinct cutoffs corresponding to each one of the semiconductors. Tauc plots of all the curves present in Figure 2 yielded for each of the cutoffs the gap energy values in Table 1. For cutoff 1, corresponding to $TiO_2$, values from 3.18 eV to 3.24 eV are obtained, the variation with the CdS contents being random. For cutoff 2 corresponding to CdS, a constant value of 2.29 ± 0.01 eV is obtained. Since the value for cutoff 1 has a larger associated error due to the superposition of CdS absorption, the values obtained may be also constant (3.21 ± 0.03 eV). This suggests that the composite is mainly made of $TiO_2$ and CdS nanoparticles, restricting the mutual interactions to the interface between them. The energy gap for cutoff 1 is close to the commonly reported value for pristine $TiO_2$ [27]. However, the one obtained for cutoff 2 is somewhat lower than the

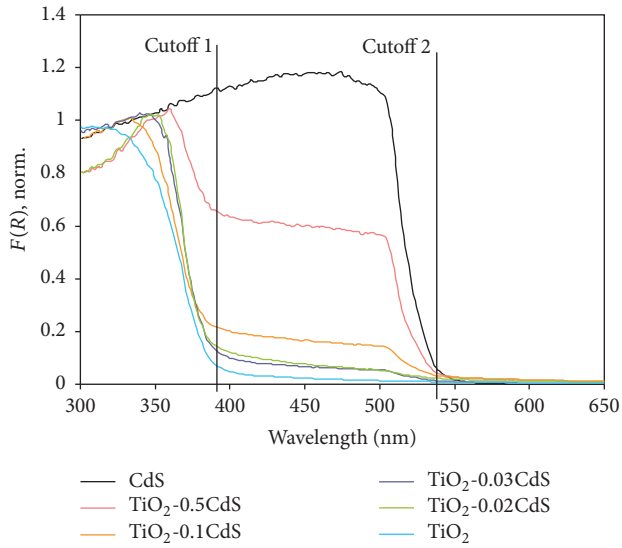


Figure 2: GSDR of all the samples under study in this work.

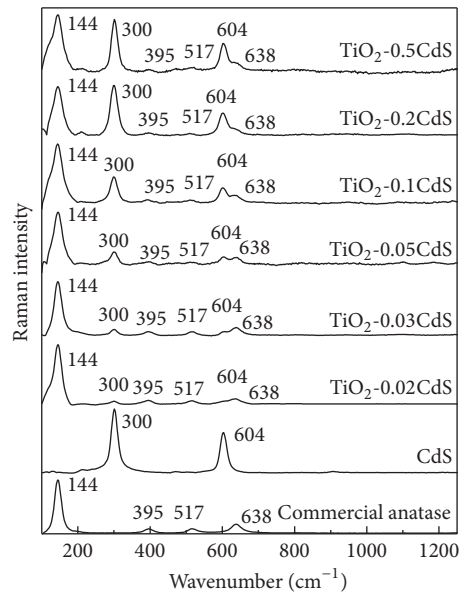


Figure 3: Raman spectra of commercial $TiO_2$ nanoparticles, $TiO_2$-*X*CdS composites, and CdS powder.

Table 1: Energy band gaps corresponding to cutoffs 1 and 2 for $TiO_2$, $TiO_2$-*X*CdS, and CdS.

| Sample | Cutoff 1 (±0.03 eV) | Cutoff 2 (±0.01 eV) |
|---|---|---|
| $TiO_2$ | 3.18 | — |
| $TiO_2$-0.02CdS | 3.22 | 2.29 |
| $TiO_2$-0.03CdS | 3.20 | 2.29 |
| $TiO_2$-0.1CdS | 3.24 | 2.29 |
| $TiO_2$-0.5CdS | 3.22 | 2.29 |
| CdS | — | 2.28 |

usually accepted value of 2.42 eV for CdS energy gap [28]. The difference is in principle due to the nanoconfinement which, in some systems, has this kind of effect.

*3.3. Raman Studies.* Well-resolved Raman peaks (Figure 3) were observed for the commercial $TiO_2$ at 144 $cm^{-1}$ ($E_g$: symmetric stretching vibration of O-Ti-O in $TiO_2$), 395 $cm^{-1}$ ($B_{1g}$: symmetric bending vibration of O-Ti-O), 517 $cm^{-1}$ ($A_{1g}$: antisymmetric bending vibration of O-Ti-O), and 638 $cm^{-1}$ ($E_g$) [29], indicating that only the anatase phase of $TiO_2$ is observed, which is in agreement with XRD analysis. As the percentage of CdS increases, the Raman spectra show a combination of the two semiconductors characteristic bands. The intensity of the bands assigned to CdS at 300 $cm^{-1}$ and 604 $cm^{-1}$ [30] increases proportionally from $TiO_2$-0.02CdS to $TiO_2$-0.5CdS. One should also note that the anatase ratio of the $E_g$ and $B_{1g}$ (or $A_{1g}$) band intensity is roughly constant with CdS content or, in other words, the three weak Raman peaks keep the same intensity ratio to the principal peak. This again suggests that both anatase and CdS crystallinity in the composite are independent of the composition.

*3.4. Laser Induced Luminescence Studies.* Figure 4 shows the laser induced luminescence spectra, all at 77 K. Figure 4(a) shows the emission of pure $TiO_2$ excited at 337 nm, Figure 4(b) is the same for the sample $TiO_2$-0.1CdS excited at 337 nm, and Figure 4(c) refers to the CdS luminescence excited at 337 nm. The $TiO_2$-0.1CdS sample excited at 410 nm, by the use of the dye laser coupled to the nitrogen laser, is presented in Figure 4(d). Figure 4(e) shows the pure CdS luminescence following excitation at 410 nm, and finally Figure 4(f) exhibits a superposition of the emission spectra obtained immediately after the laser pulse for the $TiO_2$-0.1CdS sample and for pure CdS, both excited at 410 nm. The emission of CdS peaks at about 686 nm [31] and the observed lifetime at 77 K for the pure CdS were about 575 ns. The laser induced emission spectra of undoped $TiO_2$, presented in Figure 4(a), exhibit a maximum at ~537 nm with a lifetime decay of approximately 85 ns. The important information that results from Figures 4(d) and 4(f) (from sample $TiO_2$-0.1CdS) is that luminescence from $TiO_2$ can be observed after exciting CdS at $\lambda_{exc}$ = 410 nm, where no direct excitation of $TiO_2$ occurs. This is a very important observation: the occurrence of an excitation transfer process from CdS to $TiO_2$. Although, at first sight, this seems to be an energetically impossible process to occur, it was recently reported for similar systems, namely, transfer from a plasmonic metal (donor), which is absorbed in the visible, to a semiconductor, which is absorbed in the UV (acceptor) [32, 33]. Also, a notorious increase in the lifetime of $TiO_2$ emission was observed, certainly related to the CdS longer lifetime, allowing a longer time range for the excitation transfer. The fact that it is possible to use visible light to indirectly excite $TiO_2$ is of utmost importance, since all the visible light up to ~540 nm is, in this way, useful for $TiO_2$ excitation, therefore increasing the photocatalytic activity. This greatly enhances the visible light photocatalytic activity when compared to the $TiO_2$ semiconductor alone. The fact that $TiO_2$ emission occurs following excitation of

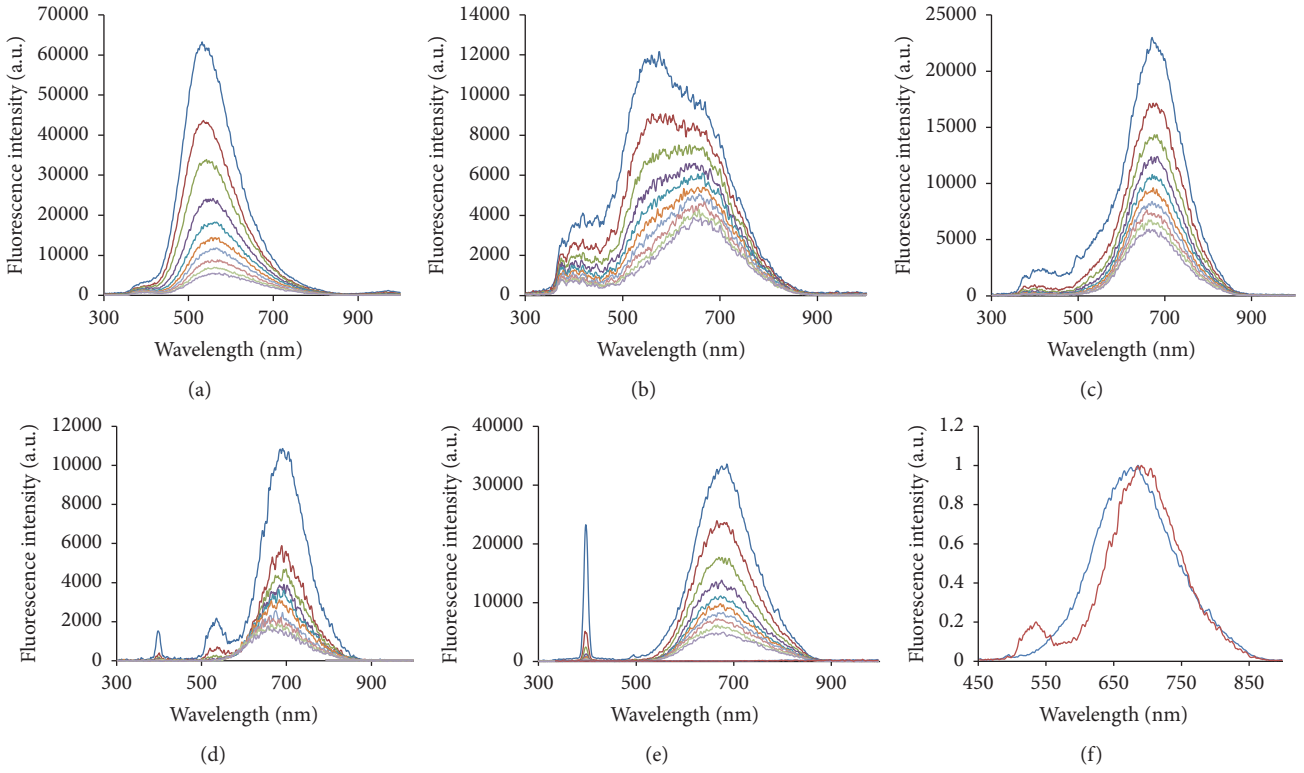


FIGURE 4: Luminescence time-resolved spectra at 77 K. The initial curve is obtained after laser pulse, and the following curves were obtained with different steps, as indicated: (a) undoped $TiO_2$ excited at 337 nm, step of 20 ns; (b) $TiO_2$-0.1CdS excited at 337 nm, step of 20 ns; (c) pure CdS excited at 337 nm, step of 100 ns; (d) $TiO_2$-0.1CdS excited at 410 nm, step of 100 ns; (e) pure CdS excited at 410 nm, step of 100 ns; (f) superposition of the normalized emission spectra obtained immediately after the laser pulse for the $TiO_2$-0.1CdS sample and pure CdS both excited at 410 nm.

CdS, while it does not occur in pure $TiO_2$ samples with visible excitation, can be clearly seen in Figure 4(d) where the time-resolved laser induced luminescence spectra clearly show a long lived emission from $TiO_2$ of about 145 ns (much larger than the one obtained with direct excitation).

*3.5. X-Ray Photoelectron Spectroscopy.* Samples with different $CdS/TiO_2$ ratios were characterized by XPS. The detailed regions corresponding to Cd 3d, S 2p, and Ti 2p are shown in Figure 5.

S 2p presents two different doublets with the main components, S $2p_{3/2}$, centred at 161.7 ± 0.3 eV and at 168.6 ± 0.2 eV, corresponding, respectively, to sulphur in CdS and in $CdSO_4$. Cd 3d includes one doublet with a spin-orbit split of ~6.8 eV. Only the main component, Cd $3d_{5/2}$, centred at 405.3 ± 0.2 eV and assigned to $Cd^{2+}$ in both CdS and $CdSO_4$ was fitted [34].

XPS (Figures 5 and 6 and Table 2) shows unequivocally that the surfaces of $TiO_2$-*X*CdS samples are composed not only of CdS, but also of oxidized sulphur, as in $CdSO_4$. The as-purchased CdS (from Aldrich) is just slightly oxidized, but in the $TiO_2$-*X*CdS catalysts, the relative amount of $SO_4^{2-}$ is not negligible the ratio $S_{(CdSO_4)}/S_{(CdS)}$ varying between ~1/3 and 1/1 (Figure 6(a)). This ratio was computed from XPS S 2p peak areas (shown in Figure 5(b)). The degree of oxidation seems to increase for $TiO_2$-*X*CdS formulations with lower overall content of CdS. Probably the degree of oxidation depends mainly on the sample surface ageing. The computed XPS ratios (Cd or S)/Ti follow a clear trend: for $TiO_2$-*X*CdS samples the experimental XPS atomic ratio Cd/Ti deviates to lower values relatively to the nominal ones especially for high nominal ratios indicating that CdS should be aggregating. This "saturation" effect on the relative amount of CdS was also detected in Raman spectra (see, in Figure 3, the ratio between peaks centred at 604 and 638 $cm^{-1}$). The experimental XPS atomic ratio S/Ti follows the same trend as Cd/Ti.

*3.6. Photodegradation Studies*

*3.6.1. Effect of the Content of CdS.* Photocatalytic activities of the $TiO_2$-*X*CdS composites were evaluated by measuring the degradation of benzoic acid in aqueous solution under visible light irradiation. The changes in the relative concentration of benzoic acid with time of irradiation were monitored by UV-vis analysis of aliquots at regular time. No detectable benzoic acid photodegradation was evidenced in aqueous solution in the absence of photocatalysts; thus, the pollutant is stable under visible irradiation in the emission range of the lamp.

As shown in Figure 7, the decomposition of benzoic acid increases as the irradiation time increases in presence of

Table 2: Corrected binding energies (eV) and, in brackets, atomic concentration (%). Also, atomic ratios sulphate to sulphide and Cd or S to Ti are shown.

| | CdS | $TiO_2$-0.5CdS | $TiO_2$-0.2CdS | $TiO_2$-0.1CdS | $TiO_2$-0.03CdS | Assignments |
|---|---|---|---|---|---|---|
| C 1s | 285.0 [38.6] | 284.9 [24.2] | 285.0 [28.6] | 284.9 [34.6] | 284.5 [25.2] | CH aliphatic |
| | 286.7 [7.6] | 286.4 [1.9] | 286.6 [3.0] | 286.4 [3.9] | 285.9 [3.5] | C-O |
| | | 288.7 [1.4] | 289.0 [2.1] | 288.9 [2.0] | 288.7 [1.4] | C=O |
| O 1s | | 530.0 [38.3] | 530.1 [37.7] | 529.9 [33.5] | 529.7 [42.6] | $TiO_2$ |
| | 532.1 [14.4] | 531.6 [7.5] | 532.0 [5.6] | 531.8 [5.3] | 531.4 [5.1] | $SO_4^{2-}$, C=O |
| | 533.8 [3.1] | 533.1 [2.4] | 533.4 [2.8] | 533.1 [2.9] | 532.6 [2.1] | C-O |
| S $2p_{3/2}$ | 161.9 [10.5] | 161.5 [0.87] | 161.5 [0.73] | 161.5 [0.40] | 161.5 [0.12] | CdS |
| S $2p_{1/2}$ | 163.1 [5.3] | 162.7 [0.43] | 162.7 [0.36] | 162.7 [0.20] | 162.8 [0.06] | |
| S $2p_{3/2}$ | 168.5 [0.7] | 168.6 [0.47] | 168.6 [0.22] | 168.5 [0.31] | 168.7 [0.12] | $SO_4^{2-}$ |
| S $2p_{1/2}$ | 169.7 [0.3] | 169.8 [0.23] | 169.8 [0.11] | 169.7 [0.15] | 169.8 [0.06] | |
| Cd $3d_{5/2}$ | 405.3 [19.5] | 405.3 [2.1] | 405.3 [1.7] | 405.5 [0.7] | 405.7 [0.3] | CdS and $CdSO_4$ |
| Ti $2p_{3/2}$ | | 458.8 [13.9] | 458.8 [12.0] | 458.8 [10.9] | 458.8 [13.7] | $TiO_2$ |
| Ti $2p_{1/2}$ | | 464.5 [6.3] | 464.5 [5.2] | 464.5 [5.1] | 464.6 [5.8] | |
| | | | *Atomic ratio* | | | |
| $S_{(SO_4^{2-})}/S_{(CdS)}$ | 0.06 | 0.54 | 0.31 | 0.77 | 1.03 | |
| Cd/Ti | | 0.11 | 0.10 | 0.05 | 0.01 | |
| S/Ti | | 0.10 | 0.08 | 0.07 | 0.02 | |

$TiO_2$-$X$CdS catalysts. The larger photocatalytic enhancement is observed for the $TiO_2$-0.02CdS catalyst: the fitting of a monoexponential function, $C/C_0$ (%) = 100 $\exp(-t/\tau)$, to the remaining pollutant relative concentrations reveals a characteristic time of degradation ($\tau$) of 3.8 h, which corresponds to the best nonlinear least square fitting. It is interesting to observe that much slower degradation takes place in presence of a catalyst with a larger content of CdS: for $TiO_2$-0.5CdS, $\tau$ is longer than 9 h. For the intermediary relative amounts of CdS, experimental data could only be fitted with biexponential curves, $C/C_0$ (%) = $A_1 \exp(-t/\tau_1) + A_2 \exp(-t/\tau_2)$ with $A_2 = 100 - A_1$. Although the photodegradation kinetics seem to be quite fast in the first couple of hours, a very slow degradation occurs afterwards, as described by the very long characteristic times ($\tau_2$) indicated in the inserted table in Figure 7. The remaining pollutant relative concentrations do not go below 31% or 38% after 6 h of irradiation with $TiO_2$-0.1CdS or $TiO_2$-0.2CdS, respectively, while with $TiO_2$-0.02CdS it reaches 24% in the same time frame. The kinetics described by biexponential curves suggest that the availability of the catalyst adsorption sites changes with time.

The effect of CdS on the optical properties of $TiO_2$ is related to the fact that the use of CdS enlarges the wavelength response range, as demonstrated by the laser induced luminescence studies, enhancing the visible light photocatalytic activity of $TiO_2$. Additionally, also according to these studies, coupling $TiO_2$ with CdS offers a way to increase the population of excited species (hole-electron pairs), extending their lifetime and promoting, in this way, the photocatalytic activity. However, Figure 7 shows that increasing $X$ from 0.02 to 0.5 leads to much slower photodegradation. In fact, even after 6 h of irradiation, a quite large relative residual concentration (51%) of benzoic acid is detected in $TiO_2$-0.5CdS. Such behavior is most probably due to the CdS aggregation onto the surface of $TiO_2$, as inferred from XPS results, and consequent decrease of specific interface $TiO_2$/CdS.

On the other hand, the sample that shows faster kinetics of degradation is also the one that is expected to be more oxidized, that is, sample with a lower CdS loading: $TiO_2$-0.02CdS. Indeed, XPS characterization has shown the presence of $SO_4^{2-}$ in addition to $S^{2-}$ at the surface of samples, revealing that the ratio $SO_4^{2-}/S^{2-}$ increases for low CdS doping amounts. In fact, the promoting effect of $SO_4^{2-}$ on the photocatalytic activity can be understood by considering that $SO_4^{2-}$ enhances the surface acidity by inducing Brönsted and Lewis acidic sites on the $TiO_2$ surface, providing more surface sites of chemisorption for reactants and oxygen molecules [35]; moreover, these sulphate species can capture reversibly electrons induced by the incident radiation, changing the oxidation state of sulphur from $S^{6+}$ to $S^{4+}$ and vice versa, inhibiting the recombination between photogenerated electrons and holes and therefore increasing the photogenerated charge carriers lifetime [36, 37].

To conclude, the enhanced activity of these oxidized samples can be ascribed to the beneficial effect of CdS which increases the $TiO_2$ lifetime and enlarges the population of charge carriers. In addition, $SO_4^{2-}$ anions resulting from the partial oxidation of $S^{2-}$ to sulphate have been identified at the surface of the catalysts and revealed to have a positive role on the photocatalytic efficiency.

*3.6.2. Effect of Organic Pollutants.* Among all the tested photocatalysts, $TiO_2$-0.02CdS seems to present better efficiency for the degradation of benzoic acid. Therefore, the study was extended for the degradation of four other carboxylic acids having different chemical structures. As shown in

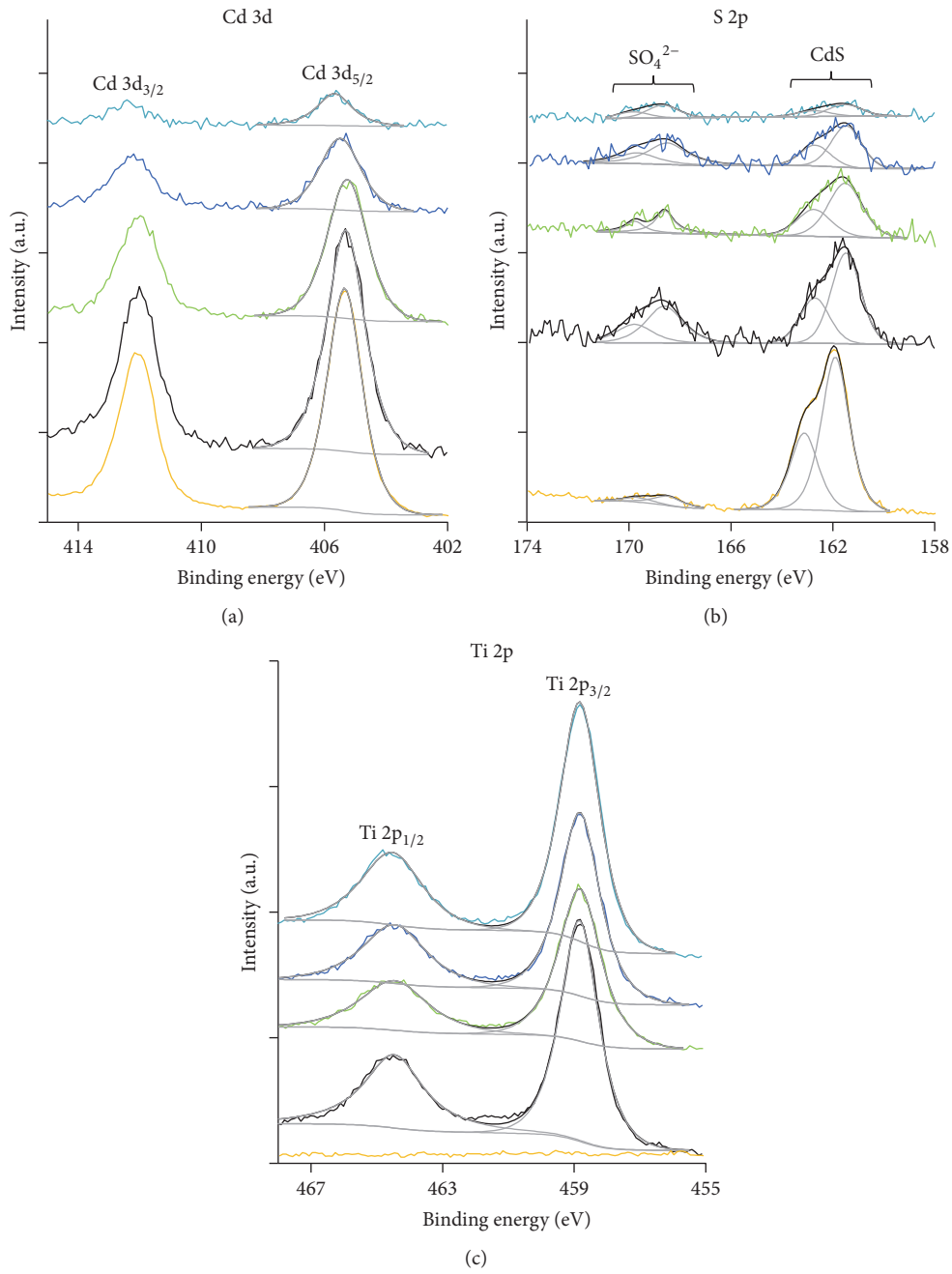


FIGURE 5: XPS Cd 3d (a), S 2p (b), and Ti 2p (c) regions, from bottom to top, of CdS (Aldrich) and $TiO_2$-$X$CdS with $X$ = 0.5, 0.2, 0.1, and 0.03 CdS.

Figure 8, $C/C_0$ depends strongly on the degraded pollutant. In the presence of $TiO_2$-0.02CdS and after 8 h of visible light irradiation, characteristic times of degradation are 3.8 h, 4.0 h, 5.8 h, 10.5 h, and 12.6 h, which lead to residual relative concentrations, after 8 h of irradiation, equal to 18%, 20%, 30%, 49%, and 58% of benzoic, salicylic, 4-bromobenzoic, 3-phenylpropionic, and veratric acids, respectively. Better performance observed for benzoic acid is probably a consequence of the high adsorption capacity of this pollutant on $TiO_2$-0.02CdS surface, which is the prerequisite step before the occurrence of the degradation process [38, 39].

*3.6.3. Reuse of the Photocatalyst.* To evaluate the photochemical stability of the catalyst, the repeated experiments for the photocatalytic decomposition of pollutant were performed using $TiO_2$-0.02CdS (freshly prepared) and $TiO_2$-0.02$CdS_{(ox)}$ (kept in air for three weeks) catalysts, and the results are presented in Figure 9.

As shown in this figure the reused samples show just a slight decrease in the photocatalytic activity. Moreover, photodegradation performance is much better using $TiO_2$-0.02$(CdS)_{ox}$ sample which emphasizes the excellent photochemical stability for both $TiO_2$-0.02CdS and

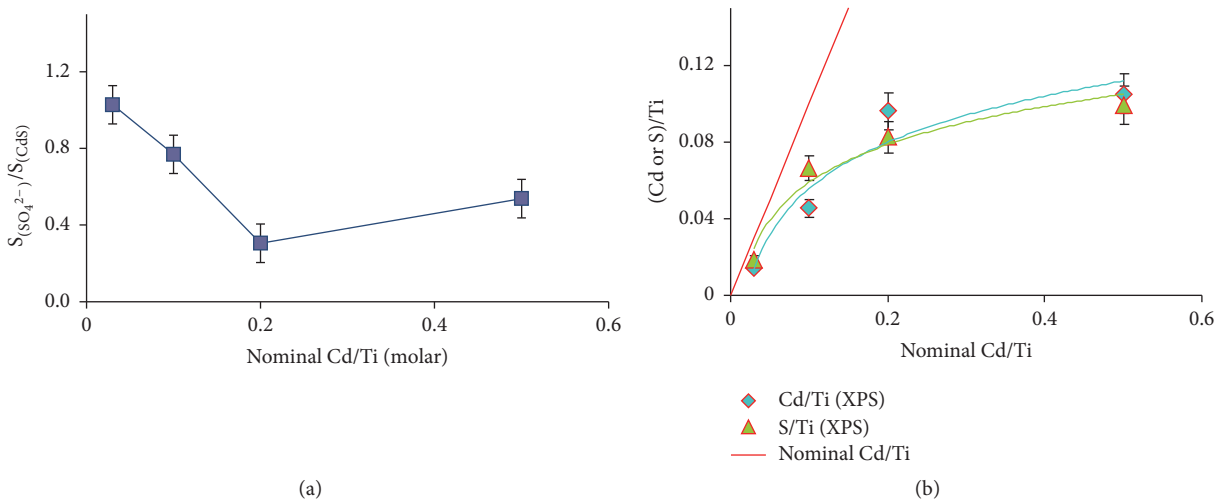


Figure 6: (a) Experimental sulphate to sulphide atomic ratio and (b) experimental atomic ratio (Cd or S)/Ti versus the Cd/Ti nominal ratio. Error bars = 10%.

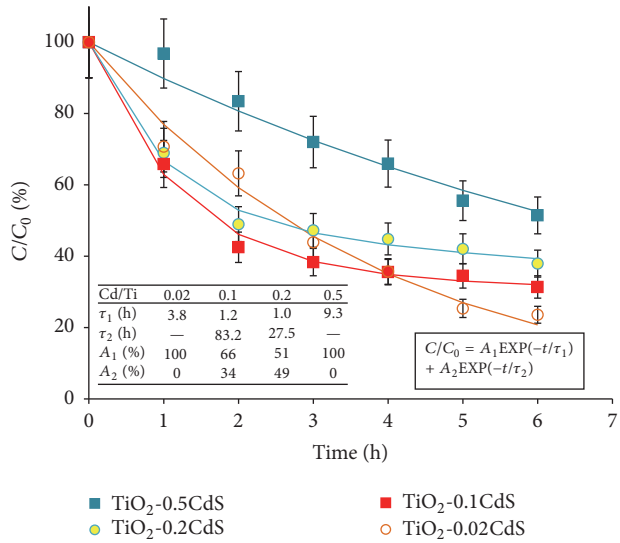


Figure 7: Effect of the CdS proportion on the photodegradation of benzoic acid under visible light irradiation. Curves correspond to the best nonlinear least square fitting of pseudomono- or pseudobiexponential functions to experimental data. The characteristic times ($\tau_1$ and $\tau_2$) that best describe the photodegradation kinetics are shown in the inserted table.

$TiO_2$-0.02$(CdS)_{ox}$ photocatalysts and confirms the beneficial role of $SO_4^{2-}$ anions. This is noteworthy from a practical application point of view as the enhanced photocatalytic activity and prevention of catalyst deactivation lead to a more cost-effective operation.

## 4. Conclusions

$TiO_2$-CdS samples with different CdS loadings were prepared to study the dependence of their photocatalytic activities on the CdS relative amount, on the degree of CdS oxidation, and on their photophysical and chemical properties.

Although GSDR does not evidence any significant change in the band gap value, both in the CdS and in the $TiO_2$ phases, the composite that shows the best photocatalytic activity under visible light is the one with a lower relative content of CdS, $TiO_2$-0.02CdS. This sample in both GSDR and Raman has spectra which are composed of the sum of $TiO_2$, in the form of anatase, and CdS. However, XPS reveals that the surfaces of $TiO_2$-CdS powders with low contents of CdS have a larger relative amount of sulphate species than samples with high CdS loads: the atomic ratios, $SO_4^{2-}/S^{2-}$, computed at the surface of $TiO_2$-0.03CdS and $TiO_2$-0.5CdS, are equal to 1.03 and 0.54, respectively. Moreover, for high doping loads, the XPS results are compatible with an aggregation of CdS, which is also confirmed by Raman, from the relative intensities of peaks centred at 604 $cm^{-1}$ and 638 $cm^{-1}$. This aggregation implies the lowering of the specific interface $TiO_2$/CdS and concomitantly the beneficial effect of CdS on the excitation of $TiO_2$ electrons through the visible light irradiation. The enhanced photocatalytic activity observed for the sample with the largest relative amount of oxidized CdS attests the beneficial role of $SO_4^{2-}$ in the photodegradation process, which is promoted by an increased surface acidity, as shown by Wang et al. [35] and others, due to the formation of a larger number of reactive surface sites enabling the chemisorption of different pollutants.

The effect of the CdS doping on the photophysics of the $TiO_2$-based photocatalysts prepared is clearly shown by the luminescence studies performed at 77 K: the laser induced emission spectra of undoped $TiO_2$ exhibit a maximum at ~537 nm, with a lifetime decay of approximately 85 ns; the emission of pure CdS peaks at about 686 nm and the observed lifetime were around 575 ns; $TiO_2$ is luminescent when the photocatalyst $TiO_2$-0.1CdS is irradiated with an excitation wavelength of 410 nm, where no direct excitation of (undoped) $TiO_2$ occurs. Such emission, which shows an important and increased lifetime of 145 ns, is the result of an excitation transfer process from CdS to $TiO_2$. The fact that it is possible to use visible light to indirectly excite $TiO_2$ is of

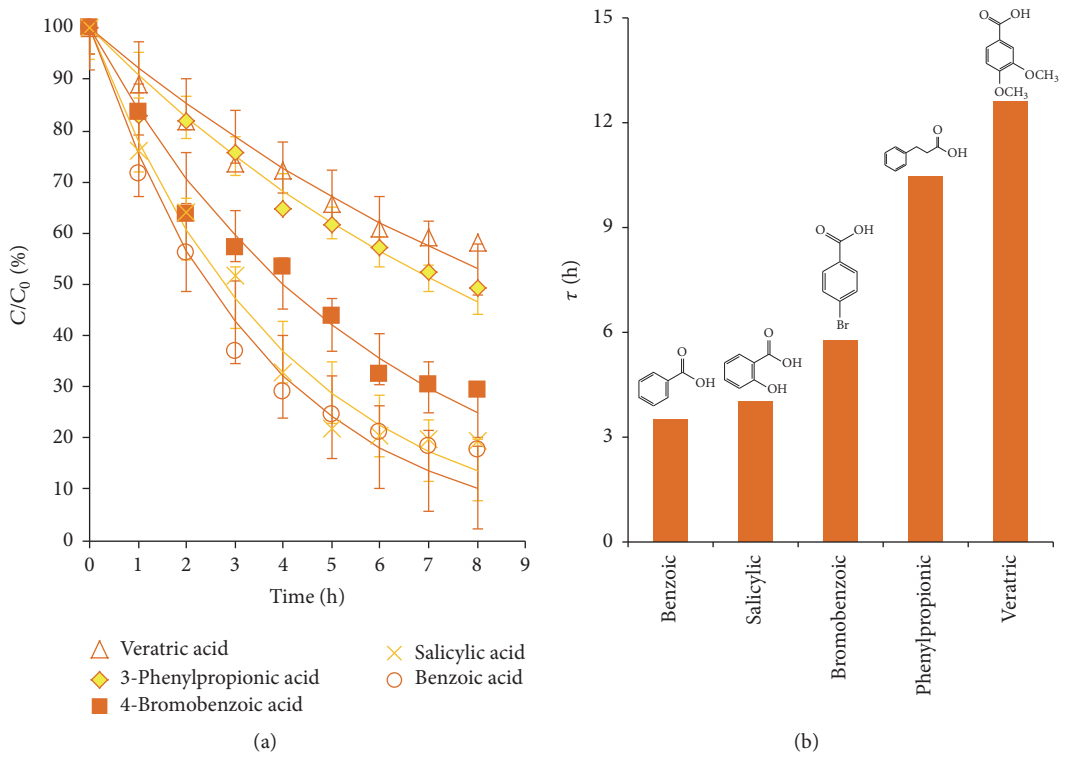


FIGURE 8: (a) Photodegradation of different carboxylic acids in the presence of $TiO_2$-0.02CdS composite under visible light irradiation. Curves correspond to the best nonlinear least square fitting of monoexponential functions to experimental data. Error bars are associated with the fitted curves and do not exceed ±8%; (b) characteristic times ($\tau$) that best describe the photodegradation kinetics.

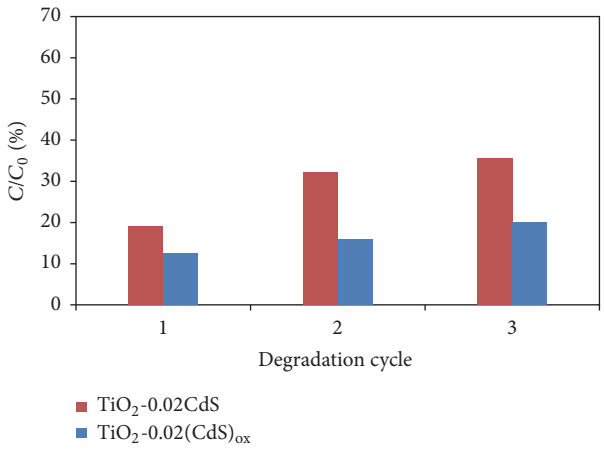


FIGURE 9: Evolution of the degradation efficiency of benzoic acid after 10 h for $TiO_2$-0.02CdS and $TiO_2$-0.02$(CdS)_{ox}$ after different degradation cycles.

utmost importance, since all the visible light up to ~540 nm is, in this way, useful for $TiO_2$ excitation therefore increasing the photocatalytic activity.

Photodegradation results show a great enhancement in the photocatalytic efficiency of the $TiO_2$-CdS composites which is due to the combined effect of the increased lifetime of the charge carriers with the relevant role of sulphate species detected at the surface. The $SO_4^{2-}$ anions may act as anchoring sites for the pollutants, therefore increasing the photocatalytic efficiency.

## Competing Interests

The authors declare that they have no competing interests.

## Acknowledgments

The authors thank the financial support granted by bilateral cooperation of "Ministère de l'Enseignement Supérieur et de la Recherche Scientifique" (Tunisia) and by FCT Project UID/NAN/50024/2013 (Portugal). A. M. Ferraria, D. P. Ferreira, D. S. Conceição, and A. P. Carapeto acknowledge FCT for the Postdoc and Ph.D. degree fellowships SFRH/BPD/108338/2015, SFRH/BD/95359/2013, SFRH/BD/95358/2013, and SFRH/BD/75734/2011.

## References

[1] A. Heller, "Conversion of sunlight into electrical power and photoassisted electrolysis of water in photoelectrochemical cells," *Accounts of Chemical Research*, vol. 14, no. 5, pp. 154–162, 1981.

[2] A. Fujishima, T. N. Rao, and D. A. Tryk, "Titanium dioxide photocatalysis," *Journal of Photochemistry and Photobiology C: Photochemistry Reviews*, vol. 1, no. 1, pp. 1–21, 2000.

[3] R. M. N. Yerga, M. C. Á. Galván, F. D. Valle, J. A. Villoria de la Mano, and J. L. G. Fierro, "Water splitting on semiconductor catalysts under visible-light irradiation," *ChemSusChem*, vol. 2, no. 6, pp. 471–485, 2009.

[4] M. Anpo and M. Takeuchi, "The design and development of highly reactive titanium oxide photocatalysts operating under visible light irradiation," *Journal of Catalysis*, vol. 216, no. 1-2, pp. 505–516, 2003.

[5] A. Di Paola, G. Marcì, L. Palmisano et al., "Preparation of polycrystalline $TiO_2$ photocatalysts impregnated with various transition metal ions: characterization and photocatalytic activity for the degradation of 4-nitrophenol," *The Journal of Physical Chemistry B*, vol. 106, no. 3, pp. 637–645, 2002.

[6] A. Di Paola, E. García-López, S. Ikeda, G. Marc, B. Ohtani, and L. Palmisano, "Photocatalytic degradation of organic compounds in aqueous systems by transition metal doped polycrystalline $TiO_2$," *Catalysis Today*, vol. 75, no. 1–4, pp. 87–93, 2002.

[7] M.-S. Kim, G. Liu, W. K. Nam, and B.-W. Kim, "Preparation of porous carbon-doped $TiO_2$ film by sol-gel method and its application for the removal of gaseous toluene in the optical fiber reactor," *Journal of Industrial and Engineering Chemistry*, vol. 17, no. 2, pp. 223–228, 2011.

[8] H. Tian, J. Ma, K. Li, and J. Li, "Hydrothermal synthesis of S-doped $TiO_2$ nanoparticles and their photocatalytic ability for degradation of methyl orange," *Ceramics International*, vol. 35, no. 3, pp. 1289–1292, 2009.

[9] D. Chatterjee and A. Mahata, "Visible light induced photodegradation of organic pollutants on dye adsorbed $TiO_2$ surface," *Journal of Photochemistry and Photobiology A: Chemistry*, vol. 153, no. 1–3, pp. 199–204, 2002.

[10] Y. Cho, W. Choi, C.-H. Lee, T. Hyeon, and H.-I. Lee, "Visible light-induced degradation of carbon tetrachloride on dye-sensitized $TiO_2$," *Environmental Science and Technology*, vol. 35, no. 5, pp. 966–970, 2001.

[11] H. Su, Y. Xie, P. Gao, Y. Xiong, and Y. Qian, "Synthesis of $MS/TiO_2$ (M = Pb, Zn, Cd) nanocomposites through a mild sol-gel process," *Journal of Materials Chemistry*, vol. 11, pp. 684–686, 2001.

[12] V. Štengl, S. Bakardjieva, N. Murafa, V. Houšková, and K. Lang, "Visible-light photocatalytic activity of $TiO_2$/ZnS nanocomposites prepared by homogeneous hydrolysis," *Microporous and Mesoporous Materials*, vol. 110, no. 2-3, pp. 370–378, 2008.

[13] W.-W. So, K.-J. Kim, and S.-J. Moon, "Photo-production of hydrogen over the $CdS\text{-}TiO_2$ nano-composite particulate films treated with $TiCl_4$," *International Journal of Hydrogen Energy*, vol. 29, no. 3, pp. 229–234, 2004.

[14] Y. Bessekhouad, N. Chaoui, M. Trzpit, N. Ghazzal, D. Robert, and J. V. Weber, "UV-vis versus visible degradation of Acid Orange II in a coupled $CdS/TiO_2$ semiconductors suspension," *Journal of Photochemistry and Photobiology A: Chemistry*, vol. 183, no. 1-2, pp. 218–224, 2006.

[15] N. Serpone, P. Maruthamuthu, P. Pichat, E. Pelizzetti, and H. Hidaka, "Exploiting the interparticle electron transfer process in the photocatalysed oxidation of phenol, 2-chlorophenol and pentachlorophenol: chemical evidence for electron and hole transfer between coupled semiconductors," *Journal of Photochemistry and Photobiology, A: Chemistry*, vol. 85, no. 3, pp. 247–255, 1995.

[16] L. Spanhel, H. Weller, and A. Henglein, "Photochemistry of semiconductor colloids. 22. Electron injection from illuminated CdS into attached $TiO_2$ and ZnO particles," *Journal of the American Chemical Society*, vol. 109, no. 22, pp. 6632–6635, 1987.

[17] H. Fujii, M. Ohtaki, K. Eguchi, and H. Arai, "Preparation and photocatalytic activities of a semiconductor composite of CdS embedded in a $TiO_2$ gel as a stable oxide semiconducting matrix," *Journal of Molecular Catalysis A: Chemical*, vol. 129, no. 1, pp. 61–68, 1998.

[18] Z. Zou, Y. Qiu, C. Xie et al., "$CdS/TiO_2$ nanocomposite film and its enhanced photoelectric responses to dry air and formaldehyde induced by visible light at room temperature," *Journal of Alloys and Compounds*, vol. 645, pp. 17–23, 2015.

[19] J.-Y. Wang, Z.-H. Liu, Q. Zheng, Z.-K. He, and R.-X. Cai, "Preparation of photosensitized nanocrystalline $TiO_2$ hydrosol by nanosized CdS at low temperature," *Nanotechnology*, vol. 17, no. 18, pp. 4561–4566, 2006.

[20] G. Colón, M. C. Hidalgo, and J. A. Navío, "Photocatalytic behaviour of sulphated $TiO_2$ for phenol degradation," *Applied Catalysis B: Environmental*, vol. 45, no. 1, pp. 39–50, 2003.

[21] X. Fu, Z. Ding, and W. Su, "Structure of titania based solid superacids and their properties for photocatalytic oxidation," *Chinese Journal of Catalysis*, vol. 20, pp. 321–324, 1999.

[22] L. F. Vieira Ferreira and I. L. Ferreira Machado, "Surface photochemistry: organic molecules within nanocavities of calixarenes," *Current Drug Discovery Technologies*, vol. 4, no. 4, pp. 229–245, 2007.

[23] L. F. Vieira Ferreira, D. S. Conceição, D. P. Ferreira, L. F. Santos, T. M. Casimiro, and I. Ferreira Machado, "Portuguese 16th century tiles from Santo António da Charneca's kiln: a spectroscopic characterization of pigments, glazes and pastes," *Journal of Raman Spectroscopy*, vol. 45, no. 9, pp. 838–847, 2014.

[24] Z. Hamden, S. Bouattour, A. Ferraria et al., "*In situ* generation of $TiO_2$ nanoparticles using chitosan as a template and their photocatalytic activity," *Journal of Photochemistry and Photobiology A: Chemistry*, vol. 321, pp. 211–222, 2016.

[25] L. Wu, J. C. Yu, and X. Fu, "Characterization and photocatalytic mechanism of nanosized CdS coupled $TiO_2$ nanocrystals under visible light irradiation," *Journal of Molecular Catalysis A: Chemical*, vol. 244, no. 1-2, pp. 25–32, 2006.

[26] Z. Hua-Yue, J. Ru, G. Yu-Jiang, F. Yong-Qian, X. Ling, and Z. Guang-Ming, "Effect of key operational factors on decolorization of methyl orange during $H_2O_2$ assisted $CdS/TiO_2$/ploymer nanocomposite thin films under simulated solar light irradiation," *Separation and Purification Technology*, vol. 74, no. 2, pp. 187–194, 2010.

[27] A. Hamdi, A. M. Ferraria, A. M. Botelho do Rego et al., "Bi–Y doped and co-doped $TiO_2$ nanoparticles: characterization and photocatalytic activity under visible light irradiation," *Journal of Molecular Catalysis A: Chemical*, vol. 380, pp. 34–42, 2013.

[28] A. I. Oliva, O. Solís-Canto, R. Castro-Rodríguez, and P. Quintana, "Formation of the band gap energy on CdS thin films growth by two different techniques," *Thin Solid Films*, vol. 391, no. 1, pp. 28–35, 2001.

[29] V. Gombac, L. De Rogatis, A. Gasparotto et al., "$TiO_2$ nanopowders doped with boron and nitrogen for photocatalytic applications," *Chemical Physics*, vol. 339, no. 1–3, pp. 111–123, 2007.

[30] J. C. Tristão, F. Magalhães, P. Corio, and M. T. C. Sansiviero, "Electronic characterization and photocatalytic properties of $CdS/TiO_2$ semiconductor composite," *Journal of Photochemistry and Photobiology A: Chemistry*, vol. 181, no. 2-3, pp. 152–157, 2006.

[31] V. Smyntyna, B. Semenenko, V. Skobeeva, and N. Malushin, "Photoactivation of luminescence in CdS nanocrystals," *Beilstein Journal of Nanotechnology*, vol. 5, no. 1, pp. 355–359, 2014.

[32] Y. Pan, S. Deng, L. Polavarapu et al., "Plasmon-enhanced photocatalytic properties of $Cu_2O$ nanowire-Au nanoparticle assemblies," *Langmuir*, vol. 28, no. 33, pp. 12304–12310, 2012.

[33] S. K. Cushing, J. Li, F. Meng et al., "Photocatalytic activity enhanced by plasmonic resonant energy transfer from metal to semiconductor," *Journal of the American Chemical Society*, vol. 134, no. 36, pp. 15033–15041, 2012.

[34] A. V. Naumkin, A. Kraut-Vass, S. W. Gaarenstroom, and C. J. Powell, *NIST X-Ray Photoelectron Spectroscopy Database*, NIST Standard Reference Database 20, Version 4.1, 2012.

[35] X. Wang, J. C. Yu, P. Liu, X. Wang, W. Su, and X. Fu, "Probing of photocatalytic surface sites on $SO_4^{2-}$/ $TiO_2$ solid acids by in situ FT-IR spectroscopy and pyridine adsorption," *Journal of Photochemistry and Photobiology A: Chemistry*, vol. 179, no. 3, pp. 339–347, 2006.

[36] H. Li, G. Li, J. Zhu, and Y. Wan, "Preparation of an active $SO_4^{2-}/TiO_2$ photocatalyst for phenol degradation under supercritical conditions," *Journal of Molecular Catalysis A: Chemical*, vol. 226, no. 1, pp. 93–100, 2005.

[37] R. Sasikala, A. P. Gaikwad, V. Sudarsan, N. Gupta, and S. R. Bharadwaj, "Cubic phase indium doped cadmium sulfide dispersed on zinc oxide: enhanced photocatalytic activity for hydrogen generation from water," *Applied Catalysis A: General*, vol. 464-465, pp. 149–155, 2013.

[38] U. I. Gaya and A. H. Abdullah, "Heterogeneous photocatalytic degradation of organic contaminants over titanium dioxide: a review of fundamentals, progress and problems," *Journal of Photochemistry and Photobiology C: Photochemistry Reviews*, vol. 9, no. 1, pp. 1–12, 2008.

[39] M. Mrowetz and E. Selli, "Photocatalytic degradation of formic and benzoic acids and hydrogen peroxide evolution in $TiO_2$ and ZnO water suspensions," *Journal of Photochemistry and Photobiology A: Chemistry*, vol. 180, no. 1-2, pp. 15–22, 2006.